Journal of Solid State Chemistry 184 (2011) 1699–1706

Contents lists available at ScienceDirect

Journal of Solid State Chemistry

journal homepage: www.elsevier.com/locate/jssc

C–H···Cl relevant discrepancy on structure, magnetic and electronic conductivity of two mixed-valence $Cu^{I}Cu^{II}$ coordination polymers

Ling Shi [a], Ping Yang [a,b], Guang Huang [a], Qian Li [a], Ning Wang [c], Jian-Zhong Wu [a,*], Ying Yu [a]

[a] School of Chemistry and Environment, South China Normal University, Guangzhou 510006, China
[b] School of Chemistry and Chemical Engineering, Sun Yat-Sen University, Guangzhou 510631, China
[c] Research Institute of Tsinghua University in Shenzhen, Shenzhen 518055, China

ARTICLE INFO

Article history:
Received 17 March 2011
Received in revised form
4 May 2011
Accepted 8 May 2011
Available online 14 May 2011

Keywords:
Coordination polymer
Crystal structure
C–H···Cl hydrogen bond
Copper

ABSTRACT

Two mixed-valence $Cu^{I}Cu^{II}$ coordination polymers $[Cu^{I}Cu^{II}(qdiol)ClL]_n$ ($qdiol^{2-}$=2,3-dioxyquinoxalinate, L=2,2′-bipyridine, **1**; L=1,10-phenanthroline, **2**) were obtained in basic ethanolic solution of $CuCl_2$, 1,4-dihydro-2,3-quinoxalinedione and L under the solvothermal condition. **1** and **2** are similar in composition, but differ remarkably in structure. The coordination modes of Cu^{II}, $qdiol^{2-}$ and L are identical in both complexes. But the Cu^{I} ions are two- and three-coordinated, and the Cl^{-} ions are terminal and bridging, in **1** and **2,** respectively, which are relevant to the significantly different C–H···Cl hydrogen bonding pattern of bpy and phen. The temperature variable magnetic susceptibilities show that **1** is paramagnetic and **2** is weakly antiferromagnetic. The complex impedance spectroscopic studies indicate that both **1** and **2** are semiconductors and **2** is more conducting.

1. Introduction

Exploring the discipline of constructing metal–organic networks with tailorable structures and properties has been the major topic in crystal engineering. Stereoelectronic coordination geometry preference of transition metal centers and certain organic or metalloligand building blocks makes it possible for their self-selective assembly and leads to preparation of a great number of coordination polymers. A few transition metal elements with different oxidation states have distinct coordination preferences. The most striking instances are the Cu^{I} and Cu^{II} ions. The Cu^{I} ion prefers to adopt linear, trigonal or tetrahedral coordination geometry, whereas the Cu^{II} ion is likely to choose square planar, planar pyramidal or octahedral coordination geometry. Their charcteristics are so distinct that one can almost tell the oxidation state of a copper ion immediately from its coordination sphere. Combining the diverse binding modes of Cu^{I} and Cu^{II} ions is expected to achieve diversity of structure and property, but how to control the structures remains a synthetic challenge. While Cu^{I} and Cu^{II} salts were used simultaneously for preparing mixed valence $Cu^{I}Cu^{II}$ complexes at ambient condition [1,2], hydro- or solvothermal synthesis has recently been proved to be an effective approach to afford $Cu^{I}Cu^{II}$ coordination polymers with N-containing ligands using a Cu^{II} salt [3–13], or seldomly a Cu^{I} salt [14,15] alone as the source of both Cu^{I} and Cu^{II}, by partial reduction or oxidation, respectively.

Bridging ligands are essential in forming coordination polymers. The organic compound 1,4-dihydro-2,3-quinoxalinedione (H_2qdione), or namely 2,3-quinoxalinediol (H_2qdiol), is tautomeric and possible to adopt different coordination modes through the multiple points of ligation, but the investigation of its coordination behavior is still scarce [16–21]. Its doubly deprotonated form, $qdiol^{2-}$, has been discovered to have two kinds of bridging modes, which are 4.1111 and $3.1_1 1_1 1_2 1_3$ according to the Harris notation [22], in $[Mo_2^{II}(N,N'\text{-di-}p\text{-anisylformamidinate})_3(qdiol)]$ [19] and $[Cu_3^{II}(qdiol)_2Cl_2(DMF)_4]_n$ [17,18], respectively, as shown in Scheme 1. In the latter complex the copper atoms are all divalent and the chlorine atoms are terminal ligands.

The bidentate chelator 2,2′-bipyridine (bpy) and 1,10-phenanthroline (phen) are frequently used as ancillary terminal ligands to modulate the structural dimension in the coordination polymer construction. They are so similar in coordination behavior that their corresponding complexes (other components the same) are often isostructural [23–27]. But it has also been found that in some cases their corresponding complexes are quite different [28–30]. It was supposed most recently that the size effect of bpy and phen might be the cause for structural discrepancy of their complexes [28].

Based on the above consideration, in this work we conducted solvothermal reactions among $CuCl_2$, H_2qdiol and bpy (or phen) and successfully obtained two $Cu^{I}Cu^{II}$ mixed valence coordination polymers, which have similar composition $[Cu^{I}Cu^{II}(qdiol)ClL]_n$ (L=2,2′-bipyridine, **1**; L=1,10-phenanthroline, **2**), but display

* Corresponding author. Fax: +86 20 85211642.
E-mail address: wujzh@scnu.edu.cn (J.-Z. Wu).

0022-4596/$ - see front matter Crown Copyright © 2011 Published by Elsevier Inc. All rights reserved.
doi:10.1016/j.jssc.2011.05.016

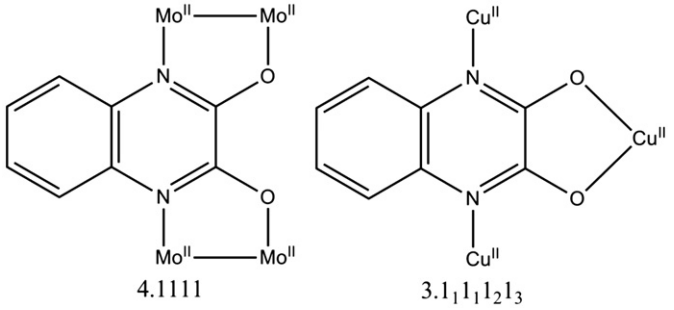

Scheme 1

significant structural differences that might be induced by the different C–H···Cl hydrogen bonding interaction patterns between C–H groups of bpy or phen and the Cl^- ion.

2. Experimental

2.1. Materials and instrumentation

The ligand H_2qdione (or H_2qdiol) was prepared according to our previously reported solid-state synthesis method [16]. All other reagents were commercially available and used as received. The infrared spectra were measured on a Perkin-Elmer Spectrum One FT-IR spectrophotometer with KBr pellets in the range of 4000–400 cm^{-1}. The C, H and N elemental analysis was performed on a Perkin-Elmer 2400 element analyzer. The magnetic susceptibility measurement was carried out for polycrystalline samples on a Quantum Design MPMS-XL5 SQUID magnetometer. Powder X-ray diffraction (PXRD) patterns were recorded on a Rigaku D/M-2200T automated diffractometer for Cu$K\alpha$ radiation (λ=1.54056 Å), with a scan speed of 4°/min and a step size of 0.02° in the 2θ range of 5–50°. Impedance measurements were conducted over a range of frequencies (0.01–10 kHz) at various temperatures (315–335 K) using a computer-controlled CHI 840B Series Precision Component Analyzer. The powder of the compound was mixed with a drop of binder material, polyvinylidene fluoride (PVDF), spreaded copper wire mesh of area 2 cm^2 and sintered at an optimized temperature (350 °C) and time (10 h) in a vacuum drying chamber before making electrical measurement.

2.2. Synthesis

*[Cu^ICu^{II}(μ-qdiol)Cl(bpy)]$_n$ (**1**)*: A solution of H_2qdiol (0.6 mmol, 0.0973 g), $CuCl_2\cdot 2H_2O$ (0.4 mmol, 0.0682 g) and bpy (0.3 mmol, 0.0469 g) in ethanol (10 ml) with pH 8 adjusted by ethanolic NaOH was put into a 23 ml Teflon-lined stainless steel reactor and heated at 140 °C for 72 h. The reaction system was cooled at a speed of 3 °C/h to 100 °C and then 5 °C/h to room temperature. Block dark green crystals were collected and washed with distilled water, yield 0.0679 g (71% based on Cu). Anal. Calcd. for $C_{18}H_{12}ClCu_2N_4O_2$: C 45.14, H 2.51, N 11.70%. Found: C 45.13, H 2.53, N 11.71%. IR (KBr, cm^{-1}): 3430*bs*, 2031*w*, 1630*m*, 1545*s*, 1487*s*, 1364*m*, 1273*w*, 1157*w*, 1090*w*, 1021*w*, 954*m*, 796*w*, 648*m*, 527*m*.

*[Cu^ICu^{II}(μ-qdiol)(μ-Cl)(phen)]$_n$ (**2**)*: The synthesis procedure is analogous to that of (**1**) except that phen (0.3 mmol, 0.0541 g) was used instead of bpy. Yield 0.0553 g (55% based on Cu). Anal. Calcd. for $C_{20}H_{12}ClCu_2N_4O_2$: C 47.76, H 2.39, N 11.14%. Found: C 47.74, H 2.38, N 11.16%. IR (KBr, cm^{-1}): 3467*bs*, 2031*w*, 1630*m*, 1529*s*, 1482*s*, 1384*m*, 1274*w*, 1157*w*, 1090*w*, 1021*w*, 954*w*, 796*w*, 648*w*, 527*w*.

Table 1
Crystallographic and structure refinement data for compounds **1** and **2**.

	1	**2**
Empiricial formula	$C_{18}H_{12}ClCu_2N_4O_2$	$C_{20}H_{12}ClCu_2N_4O_2$
Formula weight	478.87	502.89
Space group	*Ama*2	$P2_1/c$
Crystal system	Orthorhombic	Monoclinic
T (K)	293(2)	293(2)
a (Å)	13.317(2)	10.6427(14)
b (Å)	10.5909(17)	13.0324(17)
c (Å)	11.8134(19)	12.2693(16)
α (°)	90	90
β (°)	90	126.823(6)
γ (°)	90	90
V (Å^3)	1666.2(5)	1688.5(4)
Z	4	4
D_c (mg m^{-3})	1.91	1.98
M (mm^{-1})	2.74	2.71
F (000)	956	1004
Crystal size (mm^3)	0.85 × 0.80 × 0.60	0.25 × 0.24 × 0.20
θ Range for data collection	2.58–26.48	2.29–26.00
Index ranges	$-15 \le h \le 16$ $-11 \le k \le 13$ $-11 \le l \le 14$	$-11 \le h \le 13$ $-15 \le k \le 16$ $-9 \le l \le 15$
Reflections collected	4430	8508
Independent reflections	1526	3090
Data/restraints/parameters	1526/1/126	3090/0/250
Goodness-of-fit on F^2	1.03	1.06
R_1, wR_2 [$I > 2\sigma(I)$]	0.0306/0.0715	0.0613/0.1325
R_1, wR_2 (all data)	0.0361/0.0733	0.0823/0.1452
Largest difference in peak and hole (e Å^{-3})	0.415, −0.255	0.722, −0.740

2.3. X-ray crystallography

The single crystals of **1** and **2** were selected for X-ray diffraction study. Data collection was performed on a Bruker APEX II X-ray diffractometer operating with Mo$K\alpha$ radiation (λ=0.71073 Å) at room temperature. The structures were solved by the direct method and refined by full matrix least-squares on F^2 with APEX2 program. [31] All non-hydrogen atoms were refined anisotropically, and hydrogen atoms were located at their calculated positions and refined isotropically. The crystal data and structural refinement results are summarized in Table 1.

3. Results and discussion

3.1. Synthesis

Complexes **1** and **2** were successfully prepared by solvothermal reactions in ethanol. Although there are a number of reports involving hydrothermal reactions for preparing Cu^I/Cu^{II} complexes, similar reports involving solvothermal reactions, i.e. solvents other than water, are limited to three [3,12,32]. No crystalline products were obtained when water or some other organic solvents were used in our synthesis work. The IR spectra of **1** and **2** (Supplementary Materials Fig. S1) are similar and there are no strong peaks around 1700 cm^{-1} characteristic of C=O vibration as observed in [Cd(H_2qdione-κ^2O,O')(μ-Cl)$_2$]$_n$ [16], reflecting that the carbonyl coordination mode of H_2qdione is not present in complexes **1** and **2**, in agreement with the X-ray single crystal diffraction as will be discussed below.

3.2. Structural description of [Cu^ICu^{II}(μ-qdiol)Cl(bpy)]$_n$ (**1**)

X-ray analysis reveals that complex **1** crystallizes in the orthorhombic *Ama*2 space group (No. 40). This space group is

relatively rare for organic or coordination compounds. To date only 18 organic and 62 coordination compounds were found in the CCDC database to crystallize in this space group [33]. As shown in Fig. 1, there are two structurally different Cu ions. The Cu1 ion is five-coordinated with a distorted square pyramidal geometry. Two N atoms from bpy and two O atoms from $qdiol^{2-}$ are located in the symmetric square planar base, forming two 5-membered chelate rings, while a terminal Cl^- anion possesses the pyramidal apex. The Cu1 and Cl ions are situated in the crystallographic mirror plane, which bisects the bpy and $qdiol^{2-}$ ligands. The Cu2 center sits on the crystallographic two-fold axis and adopts a nearly linear geometry coordinated by two N atoms from two $qdiol^{2-}$ ligands. The selected coordination bond distances and angles are listed in Table 2. The coordination geometries strongly suggest that Cu1 and Cu2 ions are in +2 and +1 oxidation states, respectively. This conclusion is also supported by the charge balance, and bond valence sum (BVS) calculation [34–36], which shows that the calculated oxidation state values for Cu1 and Cu2 are 2.21 and 0.89, respectively.

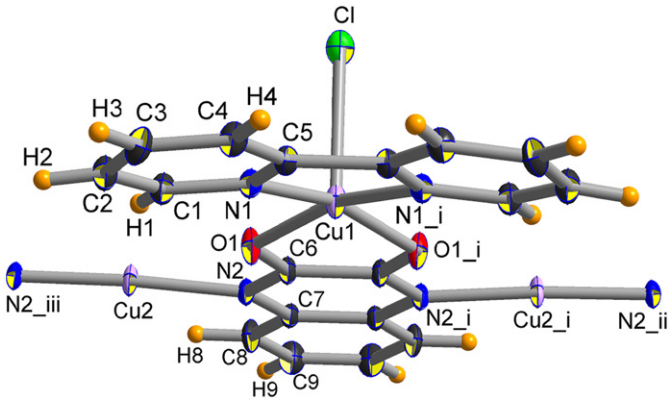

Fig. 1. An ORTEP view (30% thermal ellipsoids) of **1** showing the atom numbering scheme and coordination environments of Cu1 and Cu2. Symmetry codes: (i) $1/2-x, y, z$; (ii) $x-1/2, -y, z$; (iii) $1-x, -y, z$.

Table 2
Bond lengths and bond angle (Å and °, respectively) for complexes **1** and **2**.

Complex **1**			
Cu1–Cl	2.5073(18)	Cu1–N1^{i}	1.977(3)
Cu1–O1^{i}	1.985(3)	Cu1–O1	1.985(3)
Cu2–N2	1.908(3)	Cu2–N2^{ii}	1.908(3)
Cl–Cu1–O1	98.65(10)	Cl–Cu1–N1	97.09(10)
Cl–Cu1–O1^{i}	98.65(10)	Cl–Cu1–N1^{i}	97.09(10)
O1–Cu1–N1	95.07(12)	O1–Cu1–O1^{i}	83.97(11)
O1–Cu1–N1^{i}	164.20(14)	O1^{i}–Cu1–N1	164.20(14)
N1–Cu1–N1^{i}	81.55(13)	O1^{i}–Cu1–N1^{i}	95.07(12)
N2–Cu2–N2^{ii}	174.52(16)		
Complex **2**			
Cu1–Cl	2.689(3)	Cu1–N1	2.014(6)
Cu1–O1	1.935(4)	Cu1–N2	2.002(6)
Cu1–O2	1.951(5)	Cu2–N4	1.957(5)
Cu2–N3^{i}	1.950(4)	Cu2–Cl^{ii}	2.548(3)
Cl–Cu1–O1	93.22(18)	O2–Cu1–N1	153.1(3)
Cl–Cu1–O2	105.15(19)	O2–Cu1–N2	95.8(2)
Cl–Cu1–N1	101.70(19)	N1–Cu1–N2	81.7(2)
Cl–Cu1–N2	90.5(2)	O1–Cu1–N1	95.2(2)
O1–Cu1–O2	85.49(18)	O1–Cu1–N2	175.6(3)
N3^{i}–Cu2–N4	147.7(3)	Cl^{ii}–Cu2–N4	102.24(19)
Cl^{ii}–Cu2–N3^{ii}	110.0(2)		

Symmetry transformations used to generate equivalent atoms: (i) $-x+1/2, y, z$; (ii) $-x+1, -y, z$ for **1**; (i) $-x, y-1/2, -z+1/2$; (ii) $x, -y+1/2, z-1/2$ for **2**.

The ligand $qdiol^{2-}$ adopts μ_3-κ^4O,O',N,N' (or more precisely $3.1_1 1_1 1_2 1_3$ according to the Harris notation [22]) coordination mode, representing the second example of such coordination mode for $qdiol^{2-}$ after $[Cu^{II}_3(\mu_3\text{-qdiol-}\kappa^4O,O',N,N')_2Cl_2(DMF)_4]_n$ [17,37]. But in the latter case the Cu ions are all in +2 oxidation state, taking square planar or square pyramidal coordination geometries. In complex **1**, $qdiol^{2-}$ utilizes the two *ortho* N atoms in the pyrazine (pz) moiety to bridge two monovalent Cu2 ions with linear coordination mode (Fig. 1). Extension of this connection leads to formation of a one-dimensional (1D) infinite Cu2—pz_{qdiol}—Cu2—pz_{qdiol}⋯main chain, which is approximately linear along the *a* direction (Fig. 2). The $qdiol^{2-}$ ligands are aligned on the same side of the main chain and the neighbored $qdiol^{2-}$ ligands are inclined to each other by 31.21°. The square pyramidal polyhedra of divalent Cu1 ions are distributed alternately on the other side of the main chain.

It is interesting to observe the roles of Cl^- and bpy, which are both terminal ligands in complex **1**. The two mirror related pyridyl rings in bpy twist by 8.20°. As shown in Fig. 2 and Table 3, the chlorine ion and the C2–H2 methine groups of bpy are so close that they form intra-chain hydrogen bonds, which should be an important factor for further stabilizing the 1D chain structure and making the chain look like a cloth peg if viewing down the *a* direction (Fig. S2). There are also inter-chain C–H⋯Cl hydrogen bonds between the chlorine atom and the two symmetry related C4–H4 groups of bpy from an adjacent chain. The hydrogen bonding between the two C4–H4 groups and the chlorine atom is like a chelation pattern encodable as $R^1_2(7)$ according to the graph-set analysis [38]. The Cu−Cl coordination bond provides both charge assistance and directionality for strengthening the intra- or inter-chain C–H⋯Cl hydrogen bonds, similar to other cases involving C–H⋯Cl interactions [16,39–42]. Such inter-chain hydrogen bonds connect each 1D chain with four neighboring chains and lead to formation of a three-dimensional (3D) supramolecular network, which looks like a honeycomb with all the Cu^{I}

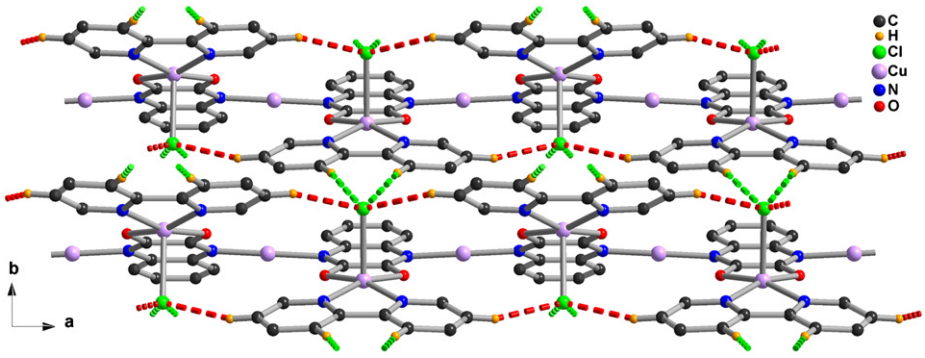

Fig. 2. Central projection of two chains of **1** illustrating the intra- (red dashed lines) and inter-chain (green dashed lines) C–H⋯Cl hydrogen bonds. The hydrogen atoms not participated in the hydrogen bonds are omitted for clarity. (For interpretation of the references to color in this figure legend, the reader is referred to the web version of this article.)

Table 3
Hydrogen bonding geometric data (Å, °) for complexes **1** and **2**.

	D–H	H···A	D···A	<D–H···A
Complex **1**				
C2–H2···Cl^{i}	0.93	2.70	3.557(4)	154
C4–H4···Cl^{ii}	0.93	2.79	3.707(4)	170
Complex **2**				
C2–H2···Cl^{i}	0.93	2.86	3.555(6)	132
C6–H6···Cl^{ii}	0.93	2.85	3.768(6)	171
C9–H9···Cl^{iii}	0.93	2.77	3.516(7)	138

Symmetry transformations used to generate equivalent atoms: (i) $1-x$, $-y$, z; (ii) x, $y+1/2$, $z+1/2$ for **1**; (i) $-x+1$, $y+1/2$, $-z+3/2$; (ii) $x+1$, $-y+1/2$, $z+1/2$; (iii) $-x+1$, $y-1/2$, $-z+3/2$ for **2**.

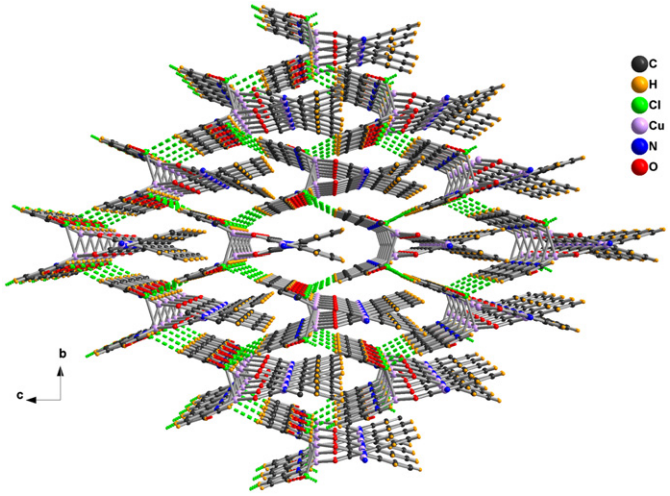

Fig. 3. Central projection of the 3D honeycomb supramolecular network of **1** constructed by inter-chain C–H···Cl hydrogen bonds (dashed lines).

ions and the qdiol ligands located inside the hexagonal prisms, as illustrated in Fig. 3.

3.3. Structural description of $[Cu^{I}Cu^{II}(\mu\text{-qdiol})(\mu\text{-Cl})(phen)]_n$ (**2**)

Complex **2** crystallizes in the common $P2_1/c$ space group. The coordination bond distances and angles are also compiled in Table 2. As illustrated in Fig. 4, the coordination mode for qdiol^{2-} and the coordination polyhedron for the Cu1 ion are the same as those in complex **1**. But compared to **1**, the coordination sphere of the Cu2 ion changes to the plane triangle. Besides the two pyrazinyl *N* atoms from two individual qdiol^{2-} ligands, the Cl^{-} ion also ligates to Cu2, acting as a bridge between Cu1 and Cu2. Calculated BVS values [34–36] for Cu1 and Cu2 ions are 2.13 and 0.94, respectively, consistent with their oxidation states and coordination polyhedra. Bridging between the Cu2 ions by pyrazine moieties of qdiol^{2-} forms zig-zag Cu2—pz_{qdiol}—Cu2—pz_{qdiol}···chains along the *b* direction. Covalent linkage of Cu1 and Cu2 ions by the chlorine atom connects the chains to form a two-dimensional (2D) covalent network, as shown in Fig. 5.

Similar to complex **1**, the C–H···Cl hydrogen bonds also play an essential role in the crystal packing in complex **2**. As shown in Table 3 and Fig. 6, each chlorine atom forms three C–H···Cl hydrogen bonds with three different phen ligands. These hydrogen bonds are nearly perpendicular to the Cu1–Cl–Cu2 line and make the adjacent 2D covalent networks intercalate into each other using their peripheral phen ligands, as illustrated in Fig. 7.

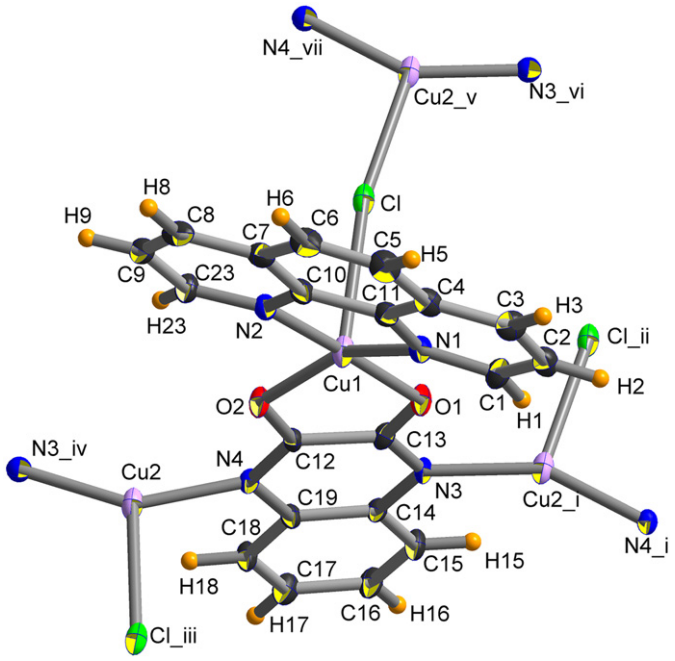

Fig. 4. An ORTEP view (30% thermal ellipsoids) of **2** showing the atom numbering scheme and coordination environments of Cu1 and Cu2. Symmetry codes: (i) $-x$, $1/2+y$, $1/2-z$; (ii) $-x$, $1-y$, $1-z$; (iii) x, $1/2-y$, $1-z$; (iv) $-x$, $-1/2+y$, $1/2-z$; (v) x, $1/2-y$, $1/2+z$; (vi) $-x$, $1-y$, $1-z$; (vii) x, $1/2-y$, $1/2+z$.

The hydrogen bonding interaction between Cl^{-} and phen ligands results in layers composed of all the organic ligands (qdiol^{2-} and phen) and the Cu ions parallel with the $(10\bar{1})$ plane. The Cu–Cl bonds function like short pillars shoring up the layers, giving rise to formation of a 3D supramolecular "pillar-layer" network (Fig. 7).

It is notable that the coordination bonds and hydrogen bonds of a Cl^{-} in either **1** or **2** sum up to 5, which seems to be the largest bonding number for Cl^{-}, as could also be found in other cases [41,43–45] although not mentioned by the authors themselves.

3.4. Bulky purity and magnetic properties

The as-isolated bulky products of complexes **1** and **2** were characterized by powder X-ray diffraction at room temperature. The experimental diffraction patterns are in agreement with the calculated diffractograms based on the single crystal data (Fig. S3), implying that the bulky samples are phase pure. The elemental analysis results also demonstrate the purity of both **1** and **2**. The crystalline samples are thus suitable for magnetic studies.

Solid-state magnetic susceptibility measurements for complexes **1** and **2** were performed in the range of 2–300 K, as shown in Fig. 8, where χ_M is the magnetic susceptibility per Cu^{II} unit. For **1**, the $\chi_M T$ value at room tempertature is 0.42 cm^3 K mol^{-1}, slightly higher than the spin-only value of 0.375 cm^3 K mol^{-1} expected for an uncoupled Cu^{II} ion ($S=1/2$, $g=2$). The $\chi_M T$ remains essentially constant in most of the temperature range and decreases slightly below 25 K and reaches 0.40 cm^3 K mol^{-1} at 2 K. The χ_M^{-1} values above 25 K can be fitted to the Curie–Weiss law, $\chi_M = C/(T-\theta)$, with Curie constant $C=0.42$ cm^3 K mol^{-1} and Weiss constant $\theta = -2.2\times10^{-3}$ K.

For complex **2**, the $\chi_M T$ value at room tempertature, 0.51 cm^3 K mol^{-1}, is higher than that of **1**. As the temperature lowered from 300 to 20 K, the $\chi_M T$ value decreased steadily from 0.51 to 0.38 cm^3 K mol^{-1}. But along with the temperature

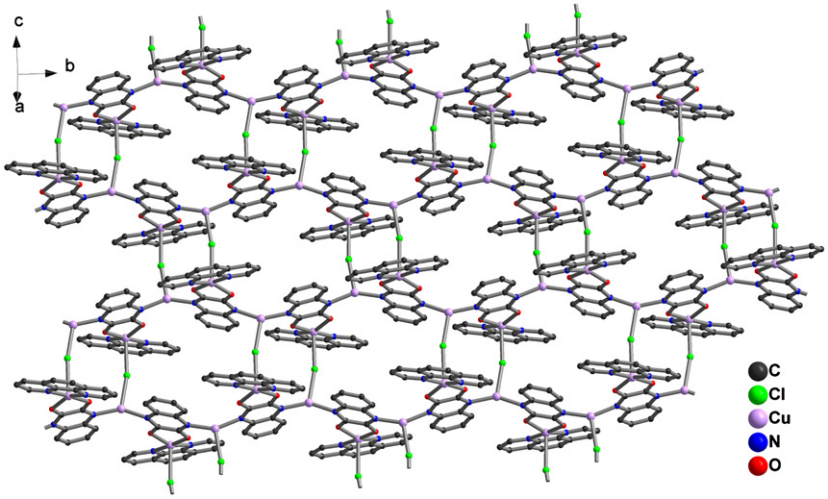

Fig. 5. Construction of the 2D covalent network in **2**.

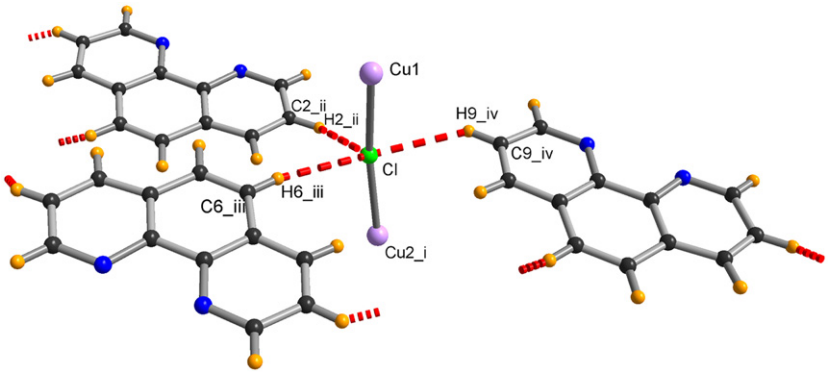

Fig. 6. Illustration of coordination bonds and C–H···Cl hydrogen bonds (dashed lines) around a chlorine atom in **2**. Symmetry codes: (i) x, $1/2-y$, $1/2+z$; (ii) $1-x$, $-1/2+y$, $1/2-z$; (iii) $-1+x$, $1/2-y$, $-1/2+z$; (iv) $1-x$, $1/2+y$, $1/2-z$.

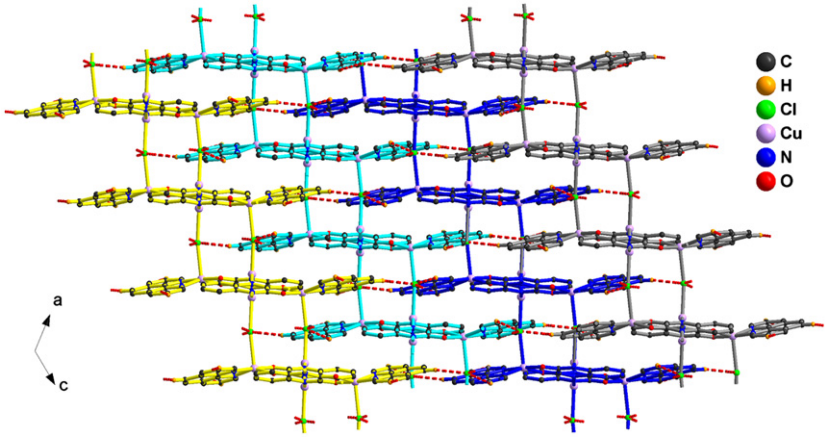

Fig. 7. 3D pillar-layer supramolecular network for **2** based on linkage of 2D covalent networks (bonds shown in different colors) by C–H···Cl hydrogen bonds (dashed lines).

continuously lowering to 2 K, the $\chi_M T$ value abruptly increased to 0.48 cm^3 K mol^{-1}. The χ_M^{-1} data do not obey the Curie–Weiss law in a large temperature range.

In both of the two complexes, the Cu^{II} paramagnetic ions are separated by diamagnetic Cu^{I} ions, which makes it possible to simulate the high-temperature magnetic susceptibilities with isotropic single-ion expression incorporating Weiss molecular field effect [46,47]:

$$\chi_M = \frac{Ng^2\beta^2}{3kT}S(S+1)$$

$$\chi = \frac{\chi_M}{1-2zj'\chi_M/Ng^2\beta^2}$$

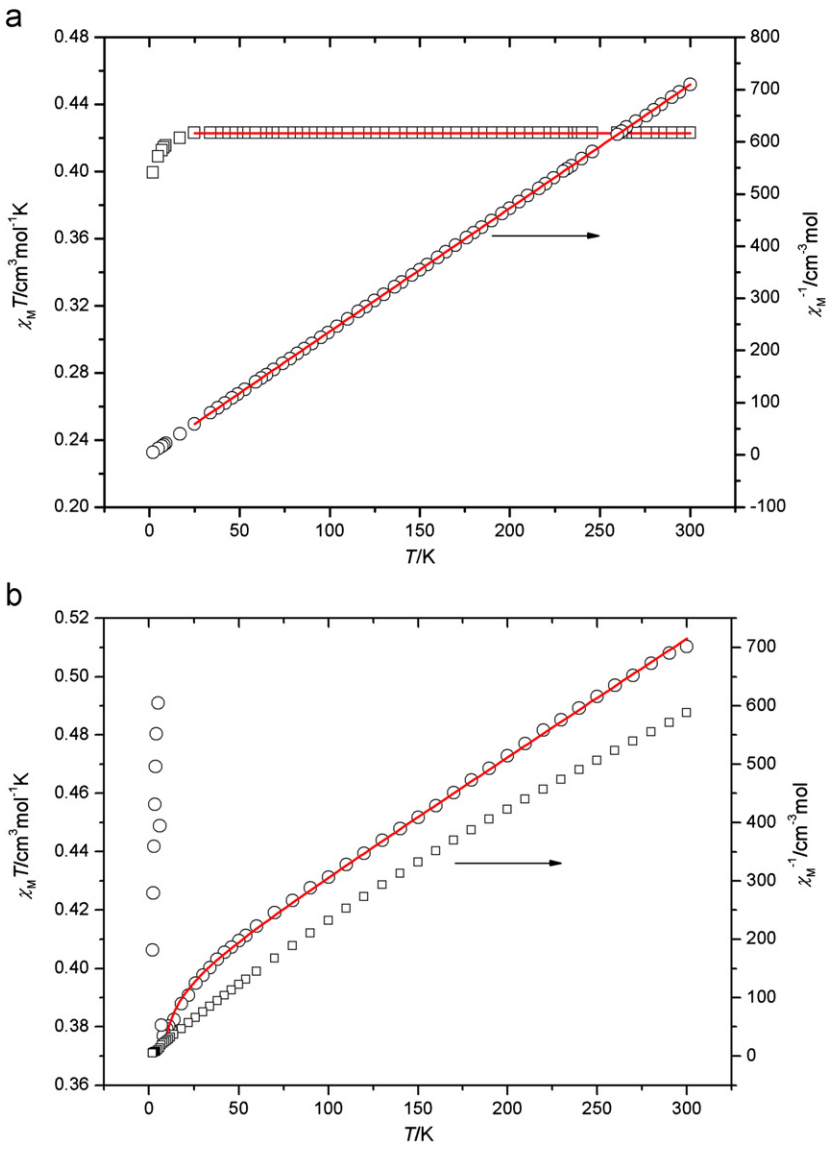

Fig. 8. Plots of χ_M^{-1} vs. T (○) and $\chi_M T$ vs. T (Δ) for **1** (a) and **2** (b). The solid lines represent the best fitting results.

where N, g, β and k have their usual meanings, zj' represents the internuclear interaction and $S=1/2$. The best fitting results (Fig. 8) are $g=2.12$, $zj'=-2.1\times10^{-3}$ cm^{-1}, $R=4.36\times10^{-5}$ for **1** and $g=2.05$, $zj'=-1.57$ cm^{-1}, $R=3.05\times10^{-5}$ for **2**, with good residue sum of squares R $(\sum(\chi_M T)_{obs.}-(\chi_M T)_{calcd.}]^2/\sum(\chi_M T)_{obs.}-(\chi_M T)_{calcd.}]^2)$. The negative zj' value for **2** implys the intermolecular antiferromagnetic coupling between the Cu^{II} cations in **2**. The small negligible value of zj', consistent with the Weiss constant, is indicative of paramagentic nature of **1**. Such magnetic behavior for **1** and **2** is consistent with their structural difference as the network in **2** is more compact than that in **1** and evidenced directly by the fact that the nearest $Cu^{II}\cdots Cu^{II}$ distance in **2** (5.709(1) Å) is significantly shorter than that in **1** (6.867(1) Å).

3.5. Electrical conductivity studies

The carrier transport property of coordination polymers is attracting attention recently although the reports are limited [2,48–50], among which only one report involves the semiconducting study of $Cu^{I}Cu^{II}$ polymers [2]. The complex impedance spectroscopy is a unique and powerful technique to characterize the electrical properties of a material. The complex impedance of "electrode/sample/electrode" configuration can be explained as the sum of a single RC (R=resistance, C=capacitance) circuit with a parallel combination. The result obtained using impedance analysis is unambiguous, and provides a true picture of the electrical behavior of the material.

Fig. 9 shows the complex impedance plots (the imaginary component Z'' versus the real component Z') of **1** and **2** at various temperatures, which are different apparently. For **1**, parts of single semicircular arcs have been observed, and the diameters of the arcs decrease with the increase of temperture, indicative of the presence of an activated conduction mechanism like a semiconductor material. For **2**, besides the behavior similar to **1**, there is also a clear indication of occurrence of second semicircles in the high frequency region.

The ZView software [51] was applied to fit the experimental data. The best equivalent circuit models for **1** and **2** are different, as shown in Fig. 10. For **1** the equivalent circuit consists of two resistances (R_1 and R_2) and one constant phase element (CPE). Whereas for **2** the equivalent circuit changes into combination of two resistances (R_1 and R_2) and two constant phase elements (CPE_1 and CPE_2) similar to the most recently reported $Cu^{I}Cu^{II}$ polymers [2]. The corresponding simulated parameters are listed

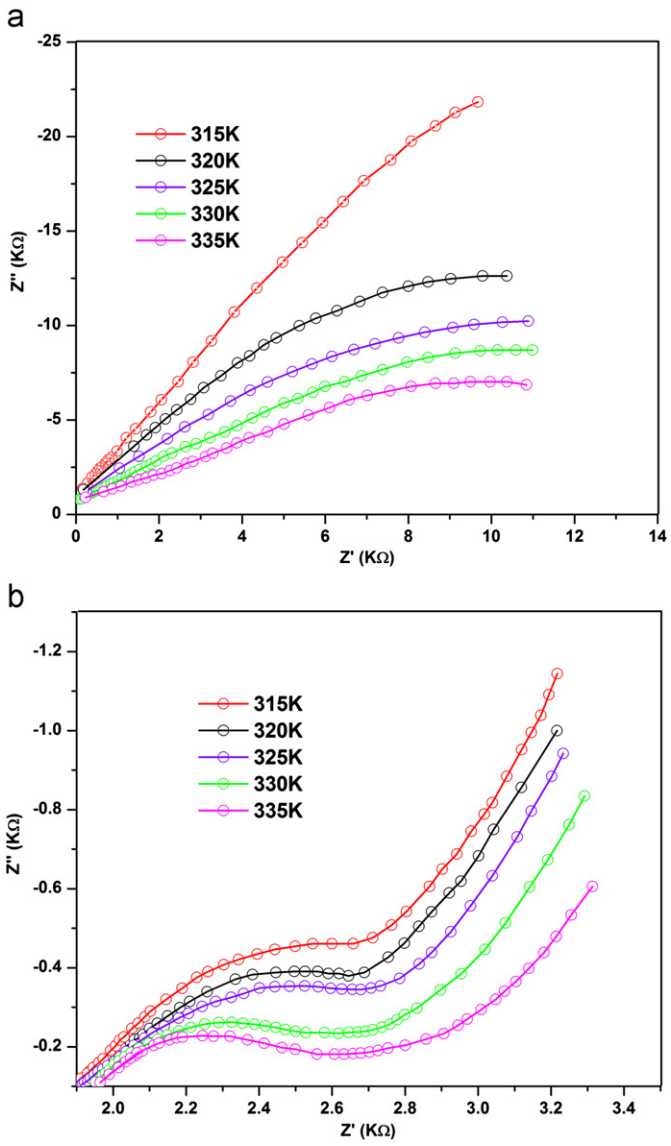

Fig. 9. Complex impedance $Z'-Z''$ plots of **1** (a) and **2** (b).

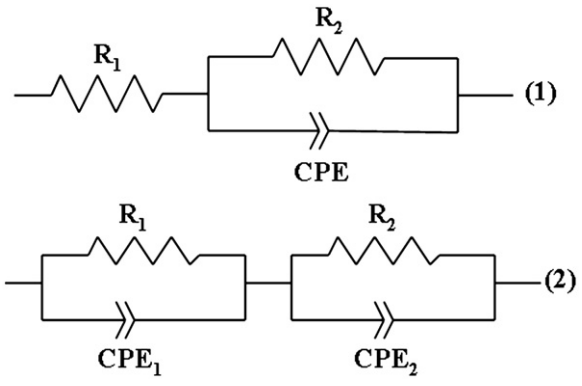

Fig. 10. The equivalent circuit models for **1** (top) and **2** (bottom).

in Table 4. The temperature relevant parameters further demonstrate the semiconductor properties of both **1** and **2**. The smaller R values in **2** than in **1** imply that the 2D coordination network of **2** is more conducting.

Table 4
Simulated parameters by fitting to the impedance data with the equivalent circuits in Fig. 10.

T (K)	Complex **1**			Complex **2**			
	R_1 (kΩ)	R_2 (kΩ)	CPE	R_1 (kΩ)	R_2 (kΩ)	CPE_1	CPE_2
315	500	500	1.00×10^{-5}	2.429	27.75	2.22×10^{-3}	2.16×10^{-4}
320	78.9	463	2.95×10^{-5}	2.021	6.73	2.34×10^{-3}	1.87×10^{-4}
325	79.8	521	2.64×10^{-5}	1.865	5.26	5.79×10^{-3}	1.76×10^{-4}
330	9.52	42.9	1.54×10^{-4}	1.844	0.969	6.69×10^{-3}	8.50×10^{-5}
335	7.46	38.6	2.88×10^{-4}	1.841	0.834	7.52×10^{-3}	3.82×10^{-5}

4. Conclusion

Utilizing 2,3-dioxyquinoxalinate as the main bridging ligand, two mixed valence $Cu^{I}Cu^{II}$ coordiantion polymers were synthesized through partial reduction of Cu^{II} to Cu^{I} under the solvothermal condition. The compositions of the two complexes are almost identical except the ancillary terminal ligands 2,2′-bipyridine and 1,10-phenanthroline. The latter two ligands differ much in forming the unconventional C–H···Cl hydrogen bonds, which may be the crucial factor for the structural distinction of the two complexes, including the disparity of coordination modes for both Cu^{I} and Cl^{-} ions, and the supramolecular networks. Consistent with the crystal structures, the magnetic and electric conducting properties of the two complexes are remarkably different.

Acknowledgments

Financial supports from the National Natural Science Foundation (Grant no. 20975041) and South China Normal University are gratefully acknowledged.

Appendix A. Supporting information

Supplementary data associated with this article can be found in the online version at doi:10.1016/j.jssc.2011.05.016.

References

[1] J.-M. Zheng, S.R. Batten, M. Du, Inorganic Chemistry 44 (2005) 3371–3373.
[2] T. Okubo, N. Tanaka, K.H. Kim, H. Yone, M. Maekawa, T. Kuroda-Sowa, Inorganic Chemistry 49 (2010) 3700.
[3] X. Xu, X. Bai, Y. Lu, E. Wang, Y. Ma, Inorganic Chemistry Communications 9 (2006) 872.
[4] E.-C. Yang, Z.-Y. Liu, X.-J. Shi, Q.-Q. Liang, X.-J. Zhao, Inorganic Chemistry 49 (2010) 7969.
[5] W. Li, M.-X. Li, M. Shao, Z.-X. Wang, H.-J. Liu, Inorganic Chemistry Communications 11 (2008) 954.
[6] H.-X. Guo, X.-Z. Li, S.-K. Huang, Y. Ling, W. Weng, Inorganic Chemistry Communications 13 (2010) 262.
[7] N.-H. Hu, Z.-G. Li, J.-W. Xu, H.-Q. Jia, J.-J. Niu, Crystal Growth & Design 7 (2007) 15.
[8] L. Hou, D. Li, W.-J. Shi, Y.-G. Yin, S.W. Ng, Inorganic Chemistry 44 (2005) 7825–7832.
[9] W. Ouellette, A.V. Prosvirin, V. Chieffo, K.R. Dunbar, B. Hudson, J. Zubieta, Inorganic Chemistry 45 (2006) 9346–9366.
[10] J. Tao, Y. Zhang, M.-L. Tong, X.-M. Chen, T. Yuen, C.L. Lin, X. Huang, J. Li, Chemical Communications (2002) 1342.
[11] X.-M. Zhang, M.-L. Tong, X.-M. Chen, Angewandte Chemie International Edition 41 (2002) 1029.
[12] X. Xu, Y. Ma, E. Wang, Inorganic Chemistry Communications 10 (2007) 1113.
[13] X.-M. Zhang, R.-Q. Fang, Inorganic Chemistry 44 (2005) 3955–3959.
[14] H. Zhao, Z.-R. Qu, Q. Ye, X.-S. Wang, J.-G. Xiong, X.-Z. You, Inorganic Chemistry 43 (2004) 1813–1815.
[15] Q. Yu, L.-G. Zhu, H.-D. Bian, J.-H. Deng, X.-G. Bao, H. Liang, Inorganic Chemistry Communications 10 (2007) 437.

[16] L. Shi, B. Cai, G. Huang, J.-Z. Wu, Y. Yu, Zeitschrift für Anorganische und Allgemeine Chemie 637 (2011) 306.
[17] K.F. Konidaris, G.S. Papaefstathiou, G. Aromi, S.J. Teat, E. Manessi-Zoupa, A. Escuer, S.P. Perlepes, Polyhedron 28 (2009) 1646.
[18] K.F. Konidaris, S.P. Perlepes, G. Aromi, S.J. Teat, A. Escuer, E. Manessi-Zoupa, Inorganic Chemistry Communications 11 (2008) 186.
[19] F.A. Cotton, J.P. Donahue, C.A. Murillo, L.M. Pérez, R. Yu, Journal of the American Chemical Society 125 (2003) 8900.
[20] M.C. Munoz, R. Ruiz, M. Traianidis, A. Aukauloo, J. Cano, Y. Journaux, I. Fernandez, J.R. Pedro, Angewandte Chemie International Edition 37 (1998) 1834.
[21] K. Yang, S.G. Bott, M.G. Richmond, Journal of Chemical Crystallography 25 (1995) 283.
[22] R.A. Coxall, S.G. Harris, D.K. Henderson, S. Parsons, P.A. Tasker, R.E.P. Winpenny, Journal of the Chemical Society, Dalton Transactions (2000) 2349.
[23] R.X. Yao, Z.M. Hao, C.H. Guo, X.M. Zhang, Crystal Engineering Communications 12 (2010) 4416.
[24] F. Costantino, A. Lenco, S. Midollini, A. Orlandini, L. Sorace, A. Vacca, European Journal of Inorganic Chemistry 19 (2008) 3046.
[25] Y.-F. Yue, J. Liang, E.-Q. Gao, C.-J. Fang, Z.-G. Yan, C.-H. Yan, Inorganic Chemistry 47 (2008) 6115.
[26] A.K. Ghosh, D. Ghoshal, E. Zangrando, J. Ribas, N.R. Chaudhuri, Inorganic Chemistry 46 (2007) 3057.
[27] D. Ghoshal, T.K. Maji, G. Mostafa, S. Sain, T.H. Lu, J. Ribas, E. Zangrando, N.R. Chaudhuri, Dalton Transactions (2004) 1687.
[28] H.L. Wang, K. Wang, D.F. Sun, Z.H. Ni, J.Z. Jiang, Crystal Engineering Communications 13 (2011) 279.
[29] V. Chandrasekhar, R. Azhakar, T. Senapati, P. Thilagar, S. Ghosh, S. Verma, R. Boomishankar, A. Steiner, P. Kogerler, Dalton Transactions (2008) 1150.
[30] M. Du, C.-P. Li, X.-J. Zhao, Q. Yu, Crystal Engineering Communications 9 (2007) 1011.
[31] Bruker, APEX2, Version 6.12 ed., Bruker AXS Inc., Madison, Wisconsin, USA, 2004.
[32] C.-P. Li, X.-H. Zhao, X.-D. Chen, Q. Yu, M. Du, Crystal Growth & Design 10 (2010) 5034.
[33] F.H. Allen, Acta Crystallographica B 58 (2002) 380.
[34] A.L. Spek, PLATON, A Multipurpose Crystallographic Tool, Utrecht University, Utrecht, The Netherlands, 2010.
[35] R.M. Wood, K.A. Abboud, R.C. Palenik, G.J. Palenik, Inorganic Chemistry 39 (2000) 2065.
[36] I.D. Brown, D. Altermatt, Acta Crystallographica B 41 (1985) 244.
[37] E. Manessi-Zoupa, K.F. Konidaris, S.P. Perlepes, G. Aromi, S.J. Teat, A. Escuer, Inorganic Chemistry Communications 11 (2008) 186.
[38] M.C. Etter, Accounts of Chemical Research 23 (1990) 120.
[39] C.B. Aakeroy, T.A. Evans, K.R. Seddon, I. Palinko, New Journal of Chemistry 23 (1999) 145.
[40] V. Balamurugan, M.S. Hundal, R. Mukherjee, Chemistry-a European Journal 10 (2004) 1683.
[41] Y.-L. Chen, B.-Z. Li, P. Yang, J.-Z. Wu, Acta Crystallographica Section C—Crystal Structure Communications 65 (2009) M238.
[42] M. Freytag, P.G. Jones, Chemical Communications (2000) 277.
[43] J.-K. Cheng, Y.-G. Yao, J. Zhang, Z.-J. Li, Z.-W. Cai, X.-Y. Zhang, Z.-N. Chen, Y.-B. Chen, Y. Kang, Y.-Y. Qin, Y.-H. Wen, Journal of American Chemical Society 126 (2004) 7796.
[44] S.H. Hong, M.W. Day, R.H. Grubbs, Journal of American Chemical Society 126 (2004) 7414.
[45] K.A. Pelz, P.S. White, M.R. Gagne, Organometallics 23 (2004) 3210.
[46] O. Kahn, Molecular Magnetism, VCH, New York, 1993.
[47] S. Cui, Y. Zhao, J. Zhang, Q. Liu, Y. Zhang, Crystal Growth & Design 8 (2008) 3803.
[48] P. Amo-Ochoa, O. Castillo, S.S. Alexandre, L. Welte, P.J. de Pablo, M.I. Rodri´guez-Tapiador, J. Go´mez-Herrero, F.I. Zamora, Inorganic Chemistry 48 (2009) 7931.
[49] S. Takaishi, M. Hosoda, T. Kajiwara, H. Miyasaka, M. Yamashita, Y. Nakanishi, Y. Kitagawa, K. Yamaguchi, A. Kobayashi, H. Kitagawa, Inorganic Chemistry 48 (2009) 9048.
[50] J.C. Zhong, Y. Misaki, M. Munakata, T. Kuroda-Sowa, M. Maekawa, Y. Suenaga, H. Konaka, Inorganic Chemistry 40 (2001) 7096.
[51] D. Johnson, A ZView, Software Program for IES Analysis, (3.1 edn.), Scribner Associates Inc., Southern Pines, NC, 2009.